Vehicle System Dynamics, 2014
Vol. 52, No. 10, 1304–1332, http://dx.doi.org/10.1080/00423114.2014.939094

Taylor & Francis
Taylor & Francis Group

Models and methodology for optimal trajectory generation in safety-critical road–vehicle manoeuvres

Karl Berntorp[a]*, Björn Olofsson[a], Kristoffer Lundahl[b] and Lars Nielsen[b]

[a]*Department of Automatic Control, Lund University, SE-221 00 Lund, Sweden;* [b]*Department of Electrical Engineering, Division of Vehicular Systems, Linköping University, SE-581 83 Linköping, Sweden*

(*Received 18 November 2013; accepted 18 June 2014*)

There is currently a strongly growing interest in obtaining optimal control solutions for vehicle manoeuvres, both in order to understand optimal vehicle behaviour and, perhaps more importantly, to devise improved safety systems, either by direct deployment of the solutions or by including mimicked driving techniques of professional drivers. However, it is non-trivial to find the right combination of models, optimisation criteria, and optimisation tools to get useful results for the above purposes. Here, a platform for investigation of these aspects is developed based on a state-of-the-art optimisation tool together with adoption of existing vehicle chassis and tyre models. A minimum-time optimisation criterion is chosen for the purpose of gaining an insight into at-the-limit manoeuvres, with the overall aim of finding improved fundamental principles for future active safety systems. The proposed method to trajectory generation is evaluated in time-manoeuvres using vehicle models established in the literature. We determine the optimal control solutions for three manoeuvres using tyre and chassis models of different complexities. The results are extensively analysed and discussed. Our main conclusion is that the tyre model has a fundamental influence on the resulting control inputs. Also, for some combinations of chassis and tyre models, inherently different behaviour is obtained. However, certain variables important in vehicle safety-systems, such as the yaw moment and the body-slip angle, are similar for several of the considered model configurations in aggressive manoeuvring situations.

Keywords: optimal manoeuvres; time-optimal trajectory generation; road vehicles; chassis and tyre modelling

1. Introduction

Optimisation of vehicle trajectories can be motivated from different perspectives. One objective is to develop improved active safety systems for standard customer cars. The Electronic Stability Control (ESC) systems, see [1,2], of today are still behind the manoeuvring performance achievable by professional rally-car drivers in situations, but the vision for improvement is there.[3] A recent survey on optimal control in automotive applications [4] points out:

> Most often, the optimal control itself will be interesting mainly insofar as it enables the discovery of the best possible system performance. Occasionally, the optimal control will provide a basis for the design and operation of practical systems.

*Corresponding author. Email: karl.berntorp@control.lth.se

Furthermore, the survey points out that finding the right balance between models, correct formulations, and optimisation methods is the fundamental problem to be solved. Moreover, the survey states that the development today is hampered by long simulation and optimisation times. However, we see that with a recent increase in computing power and advances in numerical methods for nonlinear optimisation, the simulation and optimisation times achievable today enable offline investigation of multiple model categories as well as vehicle parameters. The possibilities for online trajectory generation are still not there, mainly because of the inherent nonconvexity of the optimal control problem.

It is a common observation that time optimality in aggressive vehicle manoeuvres, combined with input and state constraints, often results in control signals utilising the achievable limits of the input and state regions. It is therefore crucial how, for example, the tyres are modelled outside their normal range of operation. In addition, chassis dynamics such as roll and pitch motion are important to give a correct representation of load transfer and vehicle stability.

The interaction between tyre and road is complex, and different tyres and roads have different characteristics.[5] Even when only considering the longitudinal stiffness, that is, the initial slope of the longitudinal force–slip (FS) curve, the experimental values differ considerably between tyres, and the variability can typically be 20–100%, see [6]. Furthermore, in addition to the differences in stiffness there are also deviations between the characteristic shape of the curve at the maximum force, where the peak can be more or less accentuated. This is illustrated for Pacejka's Magic Formula and the Highway Safety Research Institute models in [6]. The complete tyre model capturing both longitudinal and lateral forces can thus be expected to have large variability in shape and parameters, and parameter irregularity for different tyres. Moreover, the characteristics of the tyre forces depend on the road surface.[7]

1.1. *Objectives*

The objective of this paper is to utilise recent advances in optimisation tools to develop a platform for study of optimal vehicle-manoeuvring problems. The purpose is to demonstrate the usefulness of the platform, and to obtain insightful solutions where one specific interest is in future on-board systems for control and safety. Regarding methodology, this means that the control-oriented goal is to find a formulation that gives an insight into improved safety systems that benefit from the recent developments in sensor and computing power technology in vehicles; for example, future driver-assistance systems performing closer to what the most experienced drivers can do. To that end we study the time-optimal manoeuvres in three different scenarios; a 90°-turn, a hairpin turn (see Figure 1), and a double lane-change manoeuvre.

As already noted, it is stated in [4] that modelling is a crucial part. Different versions of the well-known single-track (ST) and double-track (DT) chassis models have been used in several safety systems and optimal vehicle manoeuvre studies, see [8–13] for examples with ST and [14,15] for examples with DT. An ST model sufficiently captures planar dynamics and has the advantage of lower computational complexity because of its reduced number of states. Consequently, it has greater promise for onboard systems. On the other hand, a DT model captures motion in space. In general, however, it requires more computation time when solving the corresponding optimisation problem. It is thus a natural objective to study a spectrum of chassis models and compare both the solutions and the computational burden. With the perspective of future control systems, it is natural to include the control signals, which may be the drive or brake torques on the wheels. This means that we include wheel dynamics, which is an extension of what many previous studies have done, see, for example [14–17]. Finally,

Figure 1. An example of a hairpin turn. Photo courtesy of RallySportLive.

there is the aspect of modelling of the tyre–road interaction. Such models are reproductions of the situation under which they were measured or may be an average over different conditions, and they may exhibit significant differences. Also here, aiming at onboard solutions, it is an objective to investigate a spectrum of tyre–road models from simple to more descriptive (but more computationally demanding). One especially important aspect is worth mentioning already here; model behaviour and requirements are quite different between simulation and optimisation. Even though many models have been used in simulation for many years, and shown good agreement with reality, time-optimal optimisation problems tend to result in control inputs corresponding to aggressive manoeuvring. The optimal control inputs push the models to, and even beyond, their limits, leading to non-physical behaviour. Another issue is that tyre–road models often depend on parameter fit and as such may have properties that can be managed in simulation tools, but may result in convergence to local minima and numerical instability in the optimisation, if not properly handled. All these modelling aspects are important. Thus, to demonstrate the value of a platform for studying optimal vehicle-manoeuvring problems, it must be verified that the platform provides sensible solutions for a spectrum of models with different characteristics. We have used our platform with several model combinations, and in this paper we present six different combinations of chassis and tyre models, all of which are common in the literature, and discuss and analyse the results in detail. The chosen model configurations are the ones deemed most interesting for the analysis and understanding of the balance between accuracy and computational demand for future automotive safety systems.

1.2. *Background*

Optimal control problems for vehicles in time-critical situations have been studied previously, see [8,12,18,19] for different examples concerning T-bone collisions and cornering. The influence of the road surface and the car transmission layout was investigated in [20] using an ST chassis model. Control laws for vehicle emergency manoeuvres were developed in [11] based on an analytical optimal-control approach. However, certain assumptions on the vehicle dynamics were imposed, and roll and pitch dynamics for the chassis were neglected. Optimal

lane-change manoeuvres were theoretically investigated in [21]. In particular, the minimum distance at which an approaching obstacle can be avoided was determined, given an initial speed and the optimal feasible manoeuvre. The time-optimal race-car line was investigated in [22,23], and in [4] a survey on existing vehicle dynamics applications of optimal control theory was presented. In contrast to the classical optimal control approach to vehicle manoeuvre optimisation, an approximate linearisation approach leading to a sequence of convex optimisation problems (one problem for each point in a discrete grid along the spatial path of the vehicle) was proposed in [13]. Methods for constraint-based trajectory planning for optimal manoeuvres were developed in [24,25]. In [10], the stability and agility of aggressive pendulum-turn manoeuvres, performed by professional race-car drivers, were investigated. Furthermore, Sundström et al. [14] and Andreasson [15] discussed optimal control of over-actuated vehicles, where similar optimisation tools as those employed in this paper were utilised. A method for optimal control allocation in yaw stabilisation of automotive vehicles was proposed in [16], and an expansion of the work comprising a two-level strategy for active steering and adaptive control allocation was presented in [26]. Furthermore, an optimal yaw-control law for road vehicles was discussed in [9].

The authors have previously presented a method for determining optimal manoeuvres and a subsequent comparison using different methods for tyre modelling in [27], and a comparison of optimal manoeuvres with different chassis models was treated in [28]. Moreover, we investigated the influence of the road surface on the optimal manoeuvre in [29]. Furthermore, in [30] we reported that simplified vehicle models, such as the ST model, identified from experimental data managed to replicate the behaviour of real vehicles. However, this was based on less aggressive driving situations, and not using optimisation as a criterion for determining the control inputs.

1.3. *Relation to previous work and outline*

A preliminary version of parts of the research presented here has been presented as conference contributions.[27,28] In this paper, several extensions are presented. In particular, regarding methodology, more combinations of chassis and tyres models of various complexity are investigated, and a more efficient and robust initialisation procedure to the time-optimal optimisation problem is proposed. In addition, an extensive comparison of the obtained results and a more in-depth analysis for the different manoeuvres are provided.

The rest of this paper is outlined as follows: the problem formulation and specific aim of the paper are discussed in Section 2. Vehicle and tyre modelling and the specific models investigated here are presented in Section 3, followed by the formulation and solution method for the studied time-optimal manoeuvring problem in Section 4. Optimisation results and a subsequent analysis of the obtained results are provided in Section 5. The proposed method to trajectory optimisation and the significance of the obtained results are discussed in Section 6, where conclusions also are drawn.

2. Problem formulation

The goal of the research presented in this paper is twofold. The first goal is control-oriented and consists of finding the time-optimal vehicle trajectory when manoeuvring through a time-critical situation, with the vehicle being subject to various constraints, which are motivated by physical limitations of the driver and the vehicle and the road geometry.

The second goal is model oriented and aims at investigating whether different chassis and tyre models yield fundamentally different solutions, not only in the cost function in

the optimisation but also in the internal vehicle behaviour. Of particular interest is to analyse the results from a safety-system perspective; that is, what driving behaviour and model characteristics can be extracted from the results. Hence, a part of the research is devoted to investigating how the models differ. We consider differential-algebraic equation (DAE) models of the form

$$\dot{x}(t) = G(x(t), y(t), u(t)),$$
$$0 = h(x(t), y(t), u(t)),$$

where $G(x(t), y(t), u(t))$ and $h(x(t), y(t), u(t))$ are twice continuously differentiable nonlinear functions of the vehicle differential variables x, algebraic variables y, and control inputs u, where the time dependency of the variables will be implicit in the rest of the paper. The employed vehicle models differ in both chassis and tyre aspects. We assume that the tyres stay in contact with the ground at all times. This is usually not a severe restriction for the average passenger vehicle under normal operating conditions. However, considering high-performance vehicle configurations in tight cornering, this modelling aspect would need further elaboration. The complete formulation of the optimal control problem is given in Section 4, and results in a general framework well suited for the studies performed.

3. Modelling

The vehicle dynamics modelling presented in this section incorporates the chassis motion modelling (having a varying number of degrees of freedom) and the tyre-force modelling. Furthermore, we discuss calibration of the tyre models and present a subsequent investigation of the qualitative behaviour of the studied tyre models.

3.1. *Chassis models*

We use three chassis models of different complexities. The most complex model is a DT model with roll (ϕ) and pitch (θ) dynamics and both longitudinal and lateral load transfer.[1] This chassis model is illustrated in Figure 2. The model has five degrees of freedom, namely two translational and three rotational. The chassis rotational motions in the roll, pitch, and yaw directions are characterised by the vehicle chassis inertias I_{xx}, I_{yy}, and I_{zz}, respectively. The derivation of the DT model is omitted because of space limitations; for the details we refer to [31,32]. We will, however, state the equations for the complete model in what follows.

3.1.1. *DT model*

The suspension system is modelled as a rotational spring–damper system. Consequently, the moment τ_ϕ produced by the suspension system in the roll direction is given by

$$\tau_\phi = (K_{\phi,\mathrm{f}} + K_{\phi,\mathrm{r}})\phi + (D_{\phi,\mathrm{f}} + D_{\phi,\mathrm{r}})\dot{\phi}, \tag{1}$$

and correspondingly for the moment τ_θ in the pitch direction according to

$$\tau_\theta = K_\theta \theta + D_\theta \dot{\theta}, \tag{2}$$

where K and D are parameters. Throughout the paper we use the indices f, r and $1, 2, 3, 4$ for denoting the respective wheel pair and wheel, respectively. The dynamic equations for the

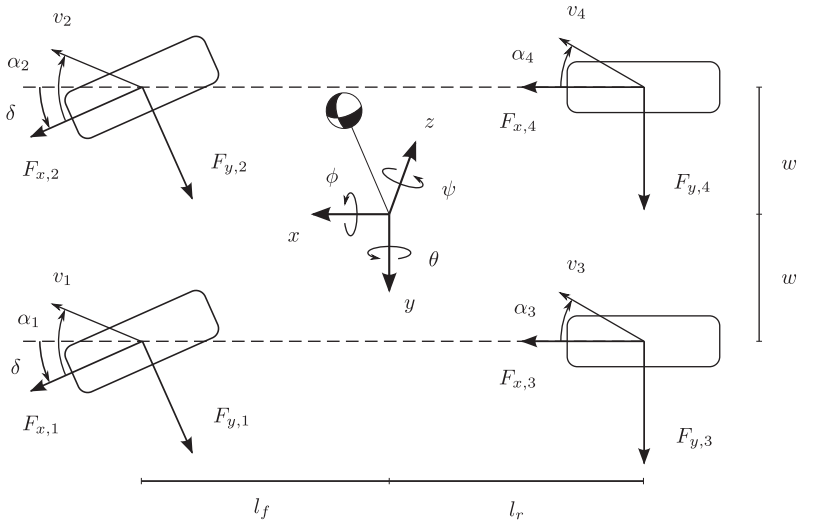

Figure 2. The DT model, with roll and pitch dynamics. Note that the geometric lateral slip angle is shown in the figure.

longitudinal load transfer are given by

$$(F_{z,1} + F_{z,2})l_{\mathrm{f}} - (F_{z,3} + F_{z,4})l_{\mathrm{r}} = K_\theta\theta + D_\theta\dot{\theta}, \quad \sum_{i=1}^{4} F_{z,i} = mg, \tag{3}$$

where $F_{z,i}$, $i \in \{1, 2, 3, 4\}$, denote the time-dependent normal forces, m is the vehicle mass, l_{f}, l_{r} are defined in Figure 2, and g is the constant of gravity. The lateral load transfer is determined by the relations

$$-w(F_{z,1} - F_{z,2}) = K_{\phi,\mathrm{f}}\phi + D_{\phi,\mathrm{f}}\dot{\phi}, \tag{4}$$

$$-w(F_{z,3} - F_{z,4}) = K_{\phi,\mathrm{r}}\phi + D_{\phi,\mathrm{r}}\dot{\phi}, \tag{5}$$

where w is defined in Figure 2.

The translational dynamic equations, which are straightforward to derive using a Newton–Euler approach, are given by

$$\begin{aligned}\dot{v}_x - v_y\dot{\psi} &= h(\sin(\theta)\cos(\phi)(\dot{\psi}^2 + \dot{\phi}^2 + \dot{\theta}^2) - \sin(\phi)\ddot{\psi} - 2\cos(\phi)\dot{\phi}\dot{\psi} \\ &\quad - \cos(\theta)\cos(\phi)\ddot{\theta} + 2\cos(\theta)\sin(\phi)\dot{\theta}\dot{\phi} + \sin(\theta)\sin(\phi)\ddot{\phi}\Big) + \frac{F_X}{m}, \\ \dot{v}_y + v_x\dot{\psi} &= h(-\sin(\theta)\cos(\phi)\ddot{\psi} - \sin(\phi)\dot{\psi}^2 - 2\cos(\theta)\cos(\phi)\dot{\theta}\dot{\psi} \\ &\quad + \sin(\theta)\sin(\phi)\dot{\phi}\dot{\psi} - \sin(\phi)\dot{\phi}^2 + \cos(\phi)\ddot{\phi}\Big) + \frac{F_Y}{m},\end{aligned}$$

where v_x, v_y are the longitudinal and lateral velocities at the mass centre, $\dot{\psi}$ is the yaw rate, and h is the distance from the roll centre to the mass centre. Moreover,

$$F_X = F_{x,1}\cos(\delta) - F_{y,1}\sin(\delta) + F_{x,2}\cos(\delta) - F_{y,2}\sin(\delta) + F_{x,3} + F_{x,4}, \tag{6}$$

$$F_Y = F_{x,1}\sin(\delta) + F_{y,1}\cos(\delta) + F_{x,2}\sin(\delta) + F_{y,2}\cos(\delta) + F_{y,3} + F_{y,4}, \tag{7}$$

where δ is the steer angle, $F_{x,i}$ is the longitudinal force for wheel i, and similarly for the lateral direction. The rotational dynamic equation for ψ is given by

$$\ddot{\psi}(I_{xx}\sin(\theta)^2+\cos(\theta)^2(I_{yy}\sin(\phi)^2+I_{zz}\cos(\phi)^2))=M_Z-h(F_X\sin(\phi)+F_Y\sin(\theta)\cos(\phi)), \tag{8}$$

where

$$\begin{aligned}M_Z=&\,l_{\mathrm{f}}(F_{x,1}\sin(\delta)+F_{x,2}\sin(\delta)+F_{y,1}\cos(\delta)+F_{y,2}\cos(\delta))\\&+w_{\mathrm{f}}(-F_{x,1}\cos(\delta)+F_{x,2}\cos(\delta)+F_{y,1}\sin(\delta)-F_{y,2}\sin(\delta))\\&-l_{\mathrm{r}}(F_{y,3}+F_{y,4})-w_{\mathrm{r}}(F_{x,3}+F_{x,4}).\end{aligned} \tag{9}$$

Note that because of the deflection of the centre of mass, the external forces in the x- and y-directions give rise to additional external torques τ_z, in this case

$$\tau_z=-h(F_X\sin(\phi)+F_Y\sin(\theta)\cos(\phi)).$$

The pitch dynamics are written as

$$\begin{aligned}\ddot{\theta}(I_{yy}\cos(\phi)^2+I_{zz}\sin(\phi)^2)=&-K_\theta\theta-D_\theta\dot{\theta}+h(mg\sin(\theta)\cos(\phi)-F_X\cos(\theta)\cos(\phi))\\&+\dot{\psi}(\dot{\psi}\sin(\theta)\cos(\theta)(\Delta I_{xy}+\cos(\phi)^2\Delta I_{yz})\\&-\dot{\phi}(\cos(\theta)^2I_{xx}+\sin(\phi)^2\sin(\theta)^2I_{yy}+\sin(\theta)^2\cos(\phi)^2I_{zz})\\&-\dot{\theta}(\sin(\theta)\sin(\phi)\cos(\phi)\Delta I_{yz})),\end{aligned} \tag{10}$$

where $\Delta I_{xy}=I_{xx}-I_{yy}$ and $\Delta I_{yz}=I_{yy}-I_{zz}$. Using $K_\phi=K_{\phi,\mathrm{f}}+K_{\phi,\mathrm{r}}$ and $D_\phi=D_{\phi,\mathrm{f}}+D_{\phi,\mathrm{r}}$, the third equation of angular motion equals

$$\begin{aligned}&\ddot{\phi}(I_{xx}\cos(\theta)^2+I_{yy}\sin(\theta)^2\sin(\phi)^2+I_{zz}\sin(\theta)^2\cos(\phi)^2)\\&\quad=-K_\phi\phi-D_\phi\dot{\phi}+h(F_Y\cos(\phi)\cos(\theta)+mg\sin(\phi))\\&\qquad+\dot{\psi}\Delta I_{yz}(\dot{\psi}\sin(\phi)\cos(\phi)\cos(\theta)+\dot{\phi}\sin(\theta)\sin(\phi)\cos(\phi))\\&\qquad+\dot{\psi}\dot{\theta}(\cos(\phi)^2I_{yy}+\sin(\phi)^2I_{zz}).\end{aligned} \tag{11}$$

3.1.2. *ST-pitch model*

The second model is an ST model, where we have added pitch dynamics (ST-pitch). The dynamics incorporate the same modelling of the suspension system in the pitch direction as for the DT model. The dynamic equations for this model are conceptually found from DT by lumping the left and right wheel on each axle together and setting the roll angle to zero. This results in the following equations of motion in the translational directions:

$$\begin{aligned}\dot{v}_x-v_y\dot{\psi}&=h(\sin(\theta)(\dot{\psi}^2+\dot{\theta}^2)-\cos(\theta)\ddot{\theta})+\frac{F_X}{m},\\\dot{v}_y+v_x\dot{\psi}&=-h(\sin(\theta)\ddot{\psi}+2\cos(\theta)\dot{\theta}\dot{\psi})+\frac{F_Y}{m},\end{aligned}$$

and the following in the rotational directions:

$$\begin{aligned}(I_{zz}+I_{xx}\sin(\theta)^2)\ddot{\psi}&=M_Z-h\sin(\theta)F_Y,\\\ddot{\theta}I_{yy}+D_\theta\dot{\theta}+K_\theta\theta-mgh\sin(\theta)&=-h\cos(\theta)F_X+\dot{\psi}^2\sin(\theta)\cos(\theta)\Delta I_{xz},\end{aligned}$$

where $\Delta I_{xz} = I_{xx} - I_{zz}$ and F_X, F_Y, and M_Z are the lumped total forces, as opposed to Equations (6), (7), and (9). The load transfer equations in the pitch direction are given by Equation (3), where the wheel forces on each axle are lumped together for the ST-pitch chassis model.

3.1.3. *ST model*

The third model is an ST model, illustrated in Figure 3. This model lumps together the left and right wheel on each axle, and roll and pitch dynamics are neglected. Thus, the model has two translational and one rotational degrees of freedom. The model dynamics are straightforward to derive [33] and are given by

$$\dot{v}_x - v_y\dot{\psi} = \frac{1}{m}(F_{x,\mathrm{f}}\cos(\delta) + F_{x,r} - F_{y,\mathrm{f}}\sin(\delta)) = \frac{F_X}{m}, \tag{12}$$

$$\dot{v}_y + v_x\dot{\psi} = \frac{1}{m}(F_{y,\mathrm{f}}\cos(\delta) + F_{y,r} + F_{x,\mathrm{f}}\sin(\delta)) = \frac{F_Y}{m}, \tag{13}$$

$$I_{zz}\ddot{\psi} = l_{\mathrm{f}}F_{y,\mathrm{f}}\cos(\delta) - l_{\mathrm{r}}F_{y,r} + l_{\mathrm{f}}F_{x,\mathrm{f}}\sin(\delta) = M_Z, \tag{14}$$

where F_X, F_Y, and M_Z are the global forces. The nominal normal force F_{z0} resting on the respective wheel in steady state is given by

$$F_{z0,\mathrm{f}} = mg\frac{l_{\mathrm{r}}}{l}, \quad F_{z0,r} = mg\frac{l_{\mathrm{f}}}{l}, \tag{15}$$

where the wheel base is defined as $l = l_{\mathrm{f}} + l_{\mathrm{r}}$.

3.2. *Wheel and tyre modelling*

The slip angles α_i and slip ratios κ_i are defined as in [5]:

$$\dot{\alpha}_i\frac{\sigma}{v_{x,i}} + \alpha_i = -\arctan\left(\frac{v_{y,i}}{v_{x,i}}\right), \tag{16}$$

$$\kappa_i = \frac{R_w\omega_i - v_{x,i}}{v_{x,i}}, \quad i \in \{f, r\} \text{ or } \{1, 2, 3, 4\}, \tag{17}$$

where σ is the relaxation length, R_w is the wheel radius, ω_i is the wheel angular velocity for wheel i, and $v_{x,i}$ and $v_{y,i}$ are the longitudinal and lateral wheel velocities for wheel i with respect to an inertial system, expressed in the coordinate system of the wheel. The wheel dynamics,[2] necessary for slip-ratio computation, are given by

$$T_i - I_w\dot{\omega}_i - F_{x,i}R_w = 0, \quad i \in \{f, r\} \text{ or } \{1, 2, 3, 4\}. \tag{18}$$

Here, T_i is the driving/braking torque and I_w is the wheel inertia.

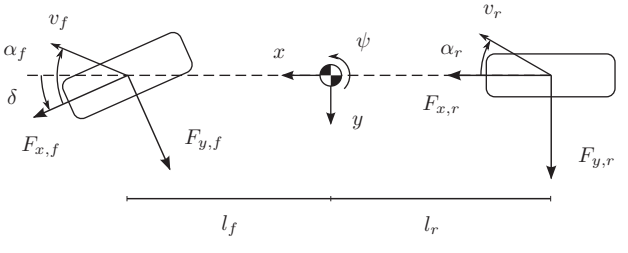

Figure 3. The ST model. Note that the geometric lateral slip angle is shown in the figure.

When developing a platform for investigation of optimal manoeuvres, it is of interest to handle and compare different tyre characteristics, and thus to cope with different tyre models. The nominal tyre forces F_{x0} and F_{y0} – that is, the forces under pure slip conditions – are computed with the Magic Formula model,[5] given by

$$F_{x0,i} = \mu_{x,i} F_{z,i} \sin(C_{x,i} \arctan(B_{x,i}\kappa_i - E_{x,i}(B_{x,i}\kappa_i - \arctan B_{x,i}\kappa_i))), \tag{19}$$

$$F_{y0,i} = \mu_{y,i} F_{z,i} \sin(C_{y,i} \arctan(B_{y,i}\alpha_i - E_{y,i}(B_{y,i}\alpha_i - \arctan B_{y,i}\alpha_i))), \tag{20}$$

for each wheel $i \in \{f, r\}$ or $\{1, 2, 3, 4\}$. In Equations (19) and (20), μ_x and μ_y are the friction coefficients and B, C, and E are model parameters.

Under combined slip conditions – that is, both κ and α are non-zero – the longitudinal and lateral tyre forces will depend on both slip quantities. How this coupling is described can have an immense effect on the vehicle dynamics. In an optimal manoeuvre, the computed control inputs will result in the best combination of longitudinal and lateral force, and these forces are, of course, coupled via the physics of the tyre. Even though detailed experiments, like the ones in [6] for longitudinal stiffness, are lacking for the complete longitudinal–lateral tyre interaction, there is a vast plethora of characteristics, see [1,5,34,35]. We have chosen two different tyre model categories for our study, which are described next.

3.2.1. *Combined forces based on the friction ellipse*

A straightforward model of combined forces is based on the friction ellipse (FE), and is described by the elliptical constraint

$$F_{y,i} = F_{y0,i}\sqrt{1 - \left(\frac{F_{x0,i}}{\mu_{x,i} F_{z,i}}\right)^2}, \quad i \in \{f, r\} \text{ or } \{1, 2, 3, 4\}, \tag{21}$$

where F_{x0} is used as an input variable, see for example.[36] However, we have opted for using the driving/braking torques as the input, see Equation (18), since this is a quantity that can be controlled in a physical set-up of a vehicle. The main limitation with the FE model is that the longitudinal force does not explicitly depend on the lateral slip, which is not realistic. With longitudinal slip present, it is possible to use a related, more involved model, which is also based on the FE.[34] However, we use Equation (21) because it represents the simplest combined-force model that is used in the vehicle optimal-control literature.[14,15] This model will hereafter be denoted as the FE model.

3.2.2. *Representing combined slip with weighting functions*

Another more comprehensive approach to tyre modelling, which is inspired by the Magic Formula and explicitly accounting for the effect on the tyre force by the longitudinal and lateral slip, is to scale the nominal forces (19) and (20) with weighting functions $G_{x\alpha,i}$ and $G_{y\kappa,i}$, which depend on α and κ.[5] The relations in the longitudinal direction are

$$H_{x\alpha,i} = B_{x1,i} \cos(\arctan(B_{x2,i}\kappa_i)), \tag{22}$$

$$G_{x\alpha,i} = \cos(C_{x\alpha,i} \arctan(H_{x\alpha,i}\alpha_i)), \tag{23}$$

$$F_{x,i} = F_{x0,i} G_{x\alpha,i}, \quad i \in \{f, r\} \text{ or } \{1, 2, 3, 4\}, \tag{24}$$

and the corresponding relations in the lateral direction are given by

$$H_{y\kappa,i} = B_{y1,i}\cos(\arctan(B_{y2,i}\alpha_i)), \tag{25}$$

$$G_{y\kappa,i} = \cos(C_{y\kappa,i}\arctan(H_{y\kappa,i}\kappa_i)), \tag{26}$$

$$F_{y,i} = F_{y0,i}G_{y\kappa,i}, \quad i \in \{f, r\} \text{ or } \{1, 2, 3, 4\}, \tag{27}$$

where B and C are model parameters. Throughout the paper, Equations (22)–(27) will be denoted by the weighting functions (WFs) model.

3.3. *Calibrating tyre models for comparison*

When comparing an optimal manoeuvre based on two different tyre models, it is not obvious how to calibrate the models with respect to the specific tyre to get comparable solutions to the optimal control problem. As an example, Figure 4 shows the resulting tyre forces for two tyre models: the first is parametrised using FE and the second is parametrised using WF. To equalise these models in comparative studies, one way would be to have the same average resultant force, whereas another way would be to equalise the longitudinal stiffness. For the particular tyre models considered in this study, the same parameters have been used in the relations for the nominal longitudinal and lateral forces in Equations (19) and (20), that is, for pure slip conditions the two tyre models agree. In the calibration procedure, we neglect that parts of the tyre model parameters which depend on the time-varying normal force; instead the parameters are determined from the normal forces present when the vehicle is in steady state.

3.3.1. *Qualitative behaviour of tyre models*

We use the FS tyre characteristic surfaces as a basis for analysis, as introduced in [27] and hereafter referred to as FS-diagrams. This 3D surface is defined as the resulting force

$$F_{\text{res},i} = \frac{\sqrt{(F_{x,i})^2 + (F_{y,i})^2}}{F_{z,i}}, \quad i \in \{f, r\} \text{ or } \{1, 2, 3, 4\}, \tag{28}$$

as a function of the longitudinal slip κ and slip angle α. The resultant is normalised with the normal force in order to enable comparison of models with and without dynamic load

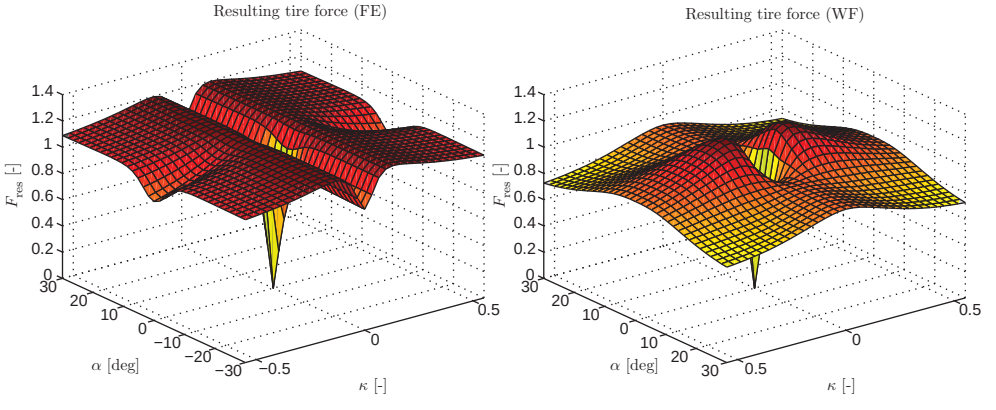

Figure 4. Resultant tyre force F_{res} for the front wheel with an FE model (left) and a WFs model (right), with experimental parameters from [5] according to Table 3. The force is normalised with the steady-state load.

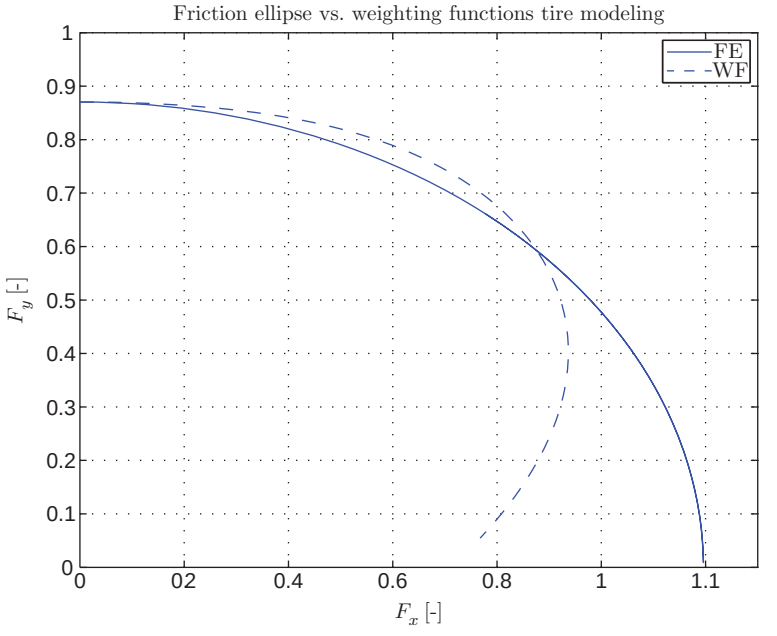

Figure 5. Lateral force plotted versus longitudinal force (normalised) for the FE and WF models, respectively, for $\alpha = 7.6^\circ$, $\kappa \in [0, 1]$. The models predict different behaviour for large values of the longitudinal force; in particular, the longitudinal force increases monotonically with decreasing lateral force for FE. Experimental results tend to support the behaviour of WF.

transfer. The model based on the WFs is parametrised according to parameters found from experiments in [5], representing a tyre behaviour when driving on dry asphalt. The FE model also uses the parameters in [5] for the nominal tyre forces. Figure 4 shows how the resulting tyre force for the front wheel varies over slip angle and slip ratio for the FE and the WFs models with the parameters presented in Table 3. Studying Figure 4 gives a basis for discussion of the behaviour of the tyre models in an optimal manoeuvre; for example, the models give different force characteristics for combined slip, where the most prominent difference is that FE predicts a significantly larger force for combined slip of high values than WF does. Furthermore, the characteristic peaks in F_{res} obviously influence the behaviour of the tyre-force model significantly.

Another fundamental difference between the models is seen in Figure 5, where the lateral force is plotted against the longitudinal force for FE and WF. Differences between the two approaches are clear. In particular, the longitudinal force increases monotonically with decreasing lateral force for FE, which is not the case for WF. Typically, experimental results exhibit similar behaviour as WF.

4. Optimal control problem

Based on the chassis and tyre dynamics described in Section 3, the time-optimal solutions for different manoeuvring situations are to be determined. These trajectories are computed as the solution to an optimisation problem and considering the physical set-up of the problem, it is clear that a solution exists given that the initial velocity of the vehicle is chosen appropriately. The resulting optimisation problems are more challenging than thought at first sight, since the time-optimality implies that the tyre-friction models operate on the boundary of their validity.

Also, solving dynamic optimisation problems numerically where the time horizon is free and is in general more demanding than solving a problem with fixed time horizon, because it adds additional degrees of freedom. Furthermore, we have found that numerical issues easily arise and that the optimisation does not converge without proper initialisation of the model trajectories prior to the optimisation. To this purpose, an initialisation procedure based on driver models has been developed as part of the optimisation platform, see Section 4.3. Moreover, scaling of the optimisation variables to the same nominal interval (based on a priori assumptions on their maximum values) is essential in order to avoid ill-conditioned matrices in the optimisation procedure.

4.1. *Formulation of the optimal control problem*

The chassis motion models presented are formulated as DAE systems according to $\dot{x} = G(x, y, u)$, as described in Section 2. The wheel driving and braking torques $T = (T_\mathrm{f}\ T_\mathrm{r})$, as well as the steer angle δ of the front wheels, are considered as inputs. For simplicity, we assume that the front wheels have the same steer angle in the DT models. Moreover, considering that the analysis in this paper has a focus on optimal manoeuvres for passenger vehicles in safety-critical situations, it is justified to assume that the DT models have one wheel-torque input for each axle. The inputs are equally distributed between the wheels at the respective axle – that is, $T_1 = T_2 = T_\mathrm{f}/2$ and $T_3 = T_4 = T_\mathrm{r}/2$. This is equivalent to separate front and rear braking systems (where, for example, anti-lock braking systems are disregarded to allow for solutions with large slip), and an open differential. Furthermore, the tyre-force model is written as the equation system $h(x, y, u) = 0$. The optimisation problem is formulated over the time horizon $t \in [0, t_\mathrm{f}]$ and the objective of the optimisation is to minimise the final time t_f of the manoeuvre. Accordingly, the dynamic optimisation problem to be solved is stated as follows:

$$
\begin{aligned}
\text{minimise} \quad & t_\mathrm{f} \\
\text{subject to} \quad & T_{i,\min} \le T_i \le T_{i,\max}, \quad i \in \{f, r\} \text{ or } \{1, 2, 3, 4\} \\
& |\dot{T}_i| \le \dot{T}_{i,\max}, \quad i \in \{f, r\} \\
& |\delta| \le \delta_{\max}, \quad |\dot{\delta}| \le \dot{\delta}_{\max} \\
& x(0) = x_0, \quad x(t_\mathrm{f}) = x_{t_\mathrm{f}}, \\
& f(X_\mathrm{p}, Y_\mathrm{p}) \le 0, \\
& \dot{x} = G(x, y, u), \quad h(x, y, u) = 0,
\end{aligned}
\tag{29}
$$

where x_0 are the initial conditions for the differential variables, x_{t_f} are the desired values for the differential variables at the final time $t = t_\mathrm{f}$, and $(X_\mathrm{p}, Y_\mathrm{p})$ is the position of the centre-of-gravity of the vehicle. In practice, the conditions at $t = t_\mathrm{f}$ are only applied to a subset of the model state variables. Furthermore, $f(X_\mathrm{p}, Y_\mathrm{p})$ is a mathematical description of the road constraint for the centre-of-gravity of the vehicle for the respective manoeuvre. These constraints in the geometric two-dimensional XY-plane are formulated as super-ellipses with different radii and degrees.

4.2. *Implementation and solution*

The chassis and tyre dynamics were implemented using the modelling language Modelica.[37] Utilising Optimica,[38] which is an extension of Modelica for high-level description of optimisation problems based on Modelica models, the implementation of the

vehicle and tyre dynamics described in Section 3 and the optimal control problem (29) was straightforward.

Because of the complex nature of the nonlinear and nonconvex optimisation problem (29), analytical solutions were intractable. Instead, we utilised numerical methods based on simultaneous collocation [39] of the continuous-time problem (29). Simultaneous collocation means that the continuous-time differential, algebraic, and control variables are discretised using an equidistant grid of the time horizon $[0, t_f]$ with N_e elements. In each element $[t_{i-1}, t_i]$, $i = 1, \ldots, N_e$, the optimisation variables are approximated using polynomials p of the format

$$p(t) = \sum_{j=1}^{N_p} p_{i,j} L_j \left(\frac{t - t_{i-1}}{h_p} \right), \quad t \in [t_{i-1}, t_i], \tag{30}$$

where $p_{i,j}$ is the interpolation coefficient, L_j is the interpolation polynomial, and h_p is the element length. Moreover, N_p collocation points are chosen in each element; in our implementation these were chosen as the corresponding Radau points. In the particular scheme employed, the differential variables were described using Lagrange polynomials of order N_c, whereas the algebraic and control variables are described using Lagrange polynomials of order $N_c - 1$. In addition, continuity of the differential variables was enforced at the element boundaries with explicit constraints in the optimisation. The collocation procedure results in a discrete-time nonlinear program (NLP), where the interpolation coefficients of the polynomials are the optimisation variables. For further details on the collocation procedure, see [40]. The resulting NLP is solved using Ipopt,[41] which is a numerical solver based on a primal–dual interior-point method opted for large and sparse optimisation problems. The collocation procedure and solution of the optimisation problem were performed using the open-source software platform JModelica.org.[42,43] For the optimisation problems considered in this paper, $N_e = 150$ discretisation elements were used and each element contained $N_c = 3$ collocation points. The selection of discretisation parameters was based on an iterative procedure. The Jacobian and the Hessian related to the problem were required in the Newton iterations in the optimisation procedure. Considering the complexity of the employed chassis and tyre models, finite-difference approximations of these quantities in quasi-Newton methods such as the Broyden–Fletcher–Goldfarb–Shanno algorithm [44] are not numerically stable, especially not for the DT model. Instead, calculation of the required derivatives with numerical precision (that is, in the order of 10^{-16}) was performed using automatic differentiation [45]; this procedure reduced convergence times several orders of magnitudes and increased numerical stability as compared with the approach using approximate derivatives.

4.3. *Initialisation procedure*

Robust convergence to a solution of the NLP in Ipopt relies on proper initialisation. We have chosen to use simulation of a driver model in combination with the vehicle model to obtain initial trajectories for the model variables in the optimisation. The driver model is designed such that the vehicle tracks the middle of the road while following a predefined velocity profile. The driver model, operating the steer angle δ and the rear-wheel torque T_r, is based on a lane-keeping controller described in [35]:

$$\delta = \delta_{ss} - k_1 e - k_2 \dot{e} - k_3 \xi - k_4 \dot{\xi}, \tag{31}$$

$$T_r = T_{r,ff} - k_5 (v - v_{nom}), \tag{32}$$

Table 1. Solution times and number of iterations required for solving the time-optimal manoeuvre problem in the hairpin turn for the considered model configurations.

Model	Solution time (s)	No. of iterations
ST FE	8.0	111
ST WF	12.3	101
ST-pitch FE	16.9	110
ST-pitch WF	7.8	78
DT FE	137.8	340
DT WF	144.2	287

where δ_{ss} is the steady-state steer angle, e is the lateral deviation from the desired path, ξ is the angular deviation from the desired heading direction, $T_{r,ff}$ is the feedforward term for the rear torque input, v_{nom} is the desired velocity profile, and $\{k_i\}_{i=1}^{5}$ are driver-model parameters. The controller parameters $k_1 - k_4$ are chosen such that the eigenvalues of the closed-loop system are placed in the same manner as suggested in [35]. The desired velocity v_{nom} is tracked by controlling the rear-wheel torques with the feedforward part $T_{r,ff}$, computed from $\dot{v}_{nom}$, and a term proportional to the speed-profile error.

The authors' experience is that the convergence time is drastically reduced when compared with the approach we utilised in [27], which was based on an iterative optimisation procedure with a sequence of smaller subproblems. Using the proposed initialisation scheme and a standard PC with an Intel Core i7 CPU in an implementation using only one of the cores, the solution times and number of iterations reported in Table 1 were obtained for the hairpin manoeuvre, which is the most challenging manoeuvre considered. Obviously, the number of iterations and computation times are dependent on the complexity of the model configuration and the manoeuvre; noticeable is that the DT chassis model requires approximately one order of magnitude longer solution time than the ST chassis model.

5. Results

In this section we present the results achieved by solving the optimal control problem (29) for different vehicle-model configurations in the different manoeuvre situations. For each investigated manoeuvre, the following chassis and tyre model configurations were evaluated:

- ST with FE for tyre modelling; that is, the ST model without pitch and roll dynamics, and the FE for tyre modelling.
- ST with WF for tyre modelling; that is, the ST model without pitch and roll dynamics, and the WFs for tyre modelling.
- ST-pitch with FE for tyre modelling; that is, the ST model with pitch dynamics, and the FE for tyre modelling.
- ST-pitch with WF for tyre modelling; that is, the ST model with pitch dynamics, and the WFs for tyre modelling.
- DT with FE for tyre modelling; that is, the DT model with pitch and roll dynamics, and the FE for tyre modelling.
- DT with WF for tyre modelling; that is, the DT model with pitch and roll dynamics, and the WFs for tyre modelling.

The numerical values for the vehicle-model parameters used in this study are provided in Table 2. The corresponding parameters for the tyre-force models are given in Table 3.

Table 2. Vehicle model parameters used in Equations (1)–(18) for the results presented in this study.

Notation	Value	Unit
l_f	1.3	m
l_r	1.5	m
w	0.8	m
m	2100	kg
I_{xx}	765	$\mathrm{kg\,m^2}$
I_{yy}	3477	$\mathrm{kg\,m^2}$
I_{zz}	3900	$\mathrm{kg\,m^2}$
R_w	0.3	m
I_w	4.0	$\mathrm{kg\,m^2}$
σ	0.3	m
g	9.82	$\mathrm{ms^{-2}}$
h	0.5	m
$K_{\phi,\mathrm{f}}, K_{\phi,\mathrm{r}}$	89,000	$\mathrm{Nm(rad)^{-1}}$
$D_{\phi,\mathrm{f}}, D_{\phi,\mathrm{r}}$	8000	$\mathrm{Nms(rad)^{-1}}$
K_θ	363,540	$\mathrm{Nm(rad)^{-1}}$
D_θ	30,960	$\mathrm{Nms(rad)^{-1}}$

Table 3. Model parameters in Equations (19)–(27) used in this study (originating from [5]).

FE	Front	Rear
μ_x	1.20	1.20
B_x	11.7	11.1
C_x	1.69	1.69
E_x	0.377	0.362
μ_y	0.935	0.961
B_y	8.86	9.30
C_y	1.19	1.19
E_y	−1.21	−1.11
WF	**Front**	**Rear**
μ_x	1.20	1.20
B_x	11.7	11.1
C_x	1.69	1.69
E_x	0.377	0.362
μ_y	0.935	0.961
B_y	8.86	9.30
C_y	1.19	1.19
E_y	−1.21	−1.11
B_{x1}	12.4	12.4
B_{x2}	−10.8	−10.8
$C_{x\alpha}$	1.09	1.09
B_{y1}	6.46	6.46
B_{y2}	4.20	4.20
$C_{y\kappa}$	1.08	1.08

Note: The models represent the tyre forces on dry asphalt with FE and WFs, respectively. For DT, the same parameters are used for both the left and the right wheels.

5.1. *Manoeuvres*

Three time manoeuvres were chosen for the evaluation of the proposed approach to trajectory generation. The motivation for choosing multiple manoeuvres is first to verify that the developed platform can handle different situations and vehicle behaviour, and second to enable comparison of the resulting solution for the considered model configurations. The first

manoeuvre is a 90°-turn, which is important in, for example, evaluation of ESC systems in lane-keeping scenarios. The second manoeuvre is a hairpin turn, which is selected because of its extremity and that it tests several aspects of the tyre and chassis modelling. The third manoeuvre is a double lane-change manoeuvre, where the dimensions of the track were chosen congruent to the ISO standard 3888-2.[46] This manoeuvre is, in particular, common for testing the possibilities for collision avoidance if obstacles are approaching the road, but is also important for the evaluation of the roll stability of a vehicle.

5.2. *Optimisation prerequisites*

For the evaluations we set the maximum allowed wheel-angle $\delta_{\max}$ and wheel-angle change rate $\dot{\delta}_{\max}$ to 30 and 60°/s, respectively, which are reasonable parameters, both seen from physical and driver limitations. For all considered manoeuvres, the start $(X_{p,0}, Y_{p,0})$ and final vehicle positions (X_{p,t_f}, Y_{p,t_f}) were set to be in the middle of the road. The initial velocities were $v_0 = 70\,\text{km/h}$ in the 90°-turn manoeuvre, $v_0 = 25\,\text{km/h}$ in the hairpin-turn manoeuvre, and $v_0 = 80\,\text{km/h}$ in the double lane-change manoeuvre. Furthermore, the lower and upper constraints on the torque inputs were chosen as

$$T_{i,\min} = -\mu_{x,i} R_w mg, \quad i \in \{f, r\} \text{ or } \{1, 2, 3, 4\}, \tag{33}$$

$$T_{r,\max} = \mu_{x,r} R_w F_{z0,r}, \tag{34}$$

$$T_{f,\max} = 0, \tag{35}$$

which implies a rear-wheel driven vehicle. The constraints on the derivative of the torque inputs were chosen as $\dot{T}_{i,\max} = 2.5\mu_{x,i} R_w mg,\ i \in \{f, r\}$. Note that the friction coefficients and the other tyre model parameters on the left and right wheels on the respective axle are assumed to be equal in the DT models. The choice of torque limitations originates from that the maximum braking torques that can be applied on the wheels are significantly larger than the corresponding acceleration torques. Furthermore, the driving torque limit was set to prevent excessive wheel spin, corresponding to large slip ratios. This is motivated since the employed empirical tyre models are based on tyre-force measurements that for experimental reasons are only possible to obtain for a limited area in the α–κ plane. The reasoning behind having constraints on the derivatives of the input torques is that the driver cannot change the acceleration or deceleration instantly, and in addition the engine or motor time constant limits the change rate of the torque in a physical vehicle. Note, however, that the choice of limitations in this paper is less restrictive than the typical values measured for a combustion engine. Moreover, the wheel velocities were limited to be nonnegative, since solutions with wheel backspin were not desired. Similarly, to aid the solver the longitudinal forces were constrained to $|F_x| \leq \mu_x F_z$ and correspondingly for the lateral forces. Note that both the force and wheel-velocity constraints are mathematically redundant.

The analysis of the achieved results presented in this section is focused on the 90°-turn and the hairpin-turn manoeuvres. The results from the double lane-change manoeuvre are commented on and compared to the results obtained for the two other manoeuvres in the discussion in Section 6.

5.3. *Optimal trajectories in 90°-turn manoeuvre*

In what follows we present an in-depth analysis of the resulting time-optimal manoeuvres for the 90°-turn. First, the computed time-optimal trajectories are explained, followed by four sections discussing different aspects of the manoeuvre; the global vehicle paths, the vehicle

model variables, the global tyre forces, and how the available tyre forces are used for the particular manoeuvres.

The vehicle start position was set to $(X_{p,0}, Y_{p,0}) = (37.5, 0)$ m, which is in the lower right corner in Figure 6, and the vehicle was aligned with the road direction, $\psi_0 = \pi/2$. The target vehicle position was set to $(X_{p,t_f}, Y_{p,t_f}) = (0, 37.5)$ m, where the vehicle heading should be in the road direction, $\psi_{t_f} = \pi$. Figure 7 displays the computed trajectories for the time-optimal manoeuvres for the different chassis and tyre model configurations in the 90°-turn. In the figure, v is the norm of the vehicle velocity vector, given by

$$v = \sqrt{v_x^2 + v_y^2},$$

and β is the body-slip angle defined as

$$\beta = \arctan\left(\frac{v_y}{v_x}\right).$$

Figure 8 shows the global forces F_X and F_Y. In addition, the yaw moment M_Z generated from the tyre forces, that is, the moment about an axis orthogonal to the road, is visualised. These quantities are displayed as a function of the driven distance s to enable comparison of the results for the different model configurations. Figures 9 and 10 show the FS-diagrams for ST with WF and DT with FE, respectively. The combination of longitudinal and lateral slip in the time-optimal solution is plotted on the surface; this gives an effective presentation of the solution. Moreover, Table 4 provides the execution times t_f for the manoeuvre with the respective model configuration. The execution times vary approximately 5% at most, which occur between the ST-pitch model with FE tyre model and DT with WF tyre models. It is noticeable that ST-pitch and DT exhibit larger discrepancies in execution times for the respective tyre model than ST. This is most certainly a result of the load transfer incorporated in the former models, which results in significant variations in the normal load on the wheels during the manoeuvre. No significant trend in the execution times is observed with regard to the chassis model. However, the FE seems to result in shorter execution times for ST-pitch and DT. This is because the resulting force for the FE is always larger than that for the WFs when combined slip is present, see Figure 4. In this manoeuvre combined slip is developed; hence, the FE results in larger forces and thus increased acceleration and deceleration.

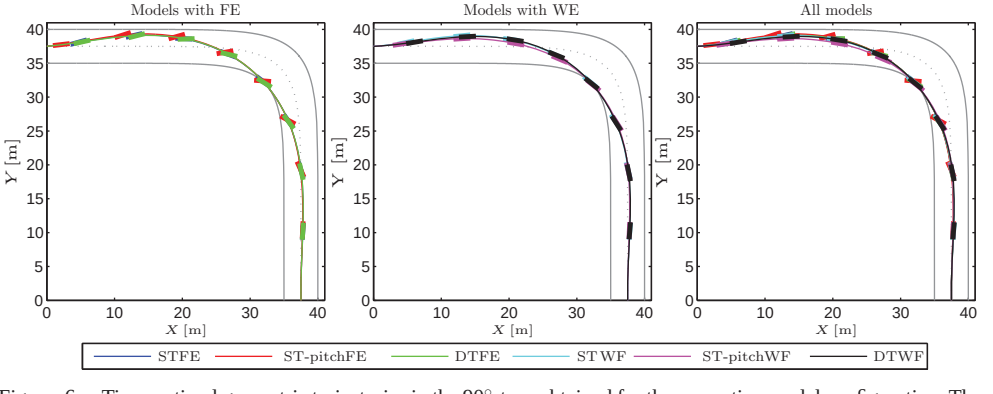

Figure 6. Time-optimal geometric trajectories in the 90°-turn obtained for the respective model configuration. The coloured bars represent the vehicle heading every half second.

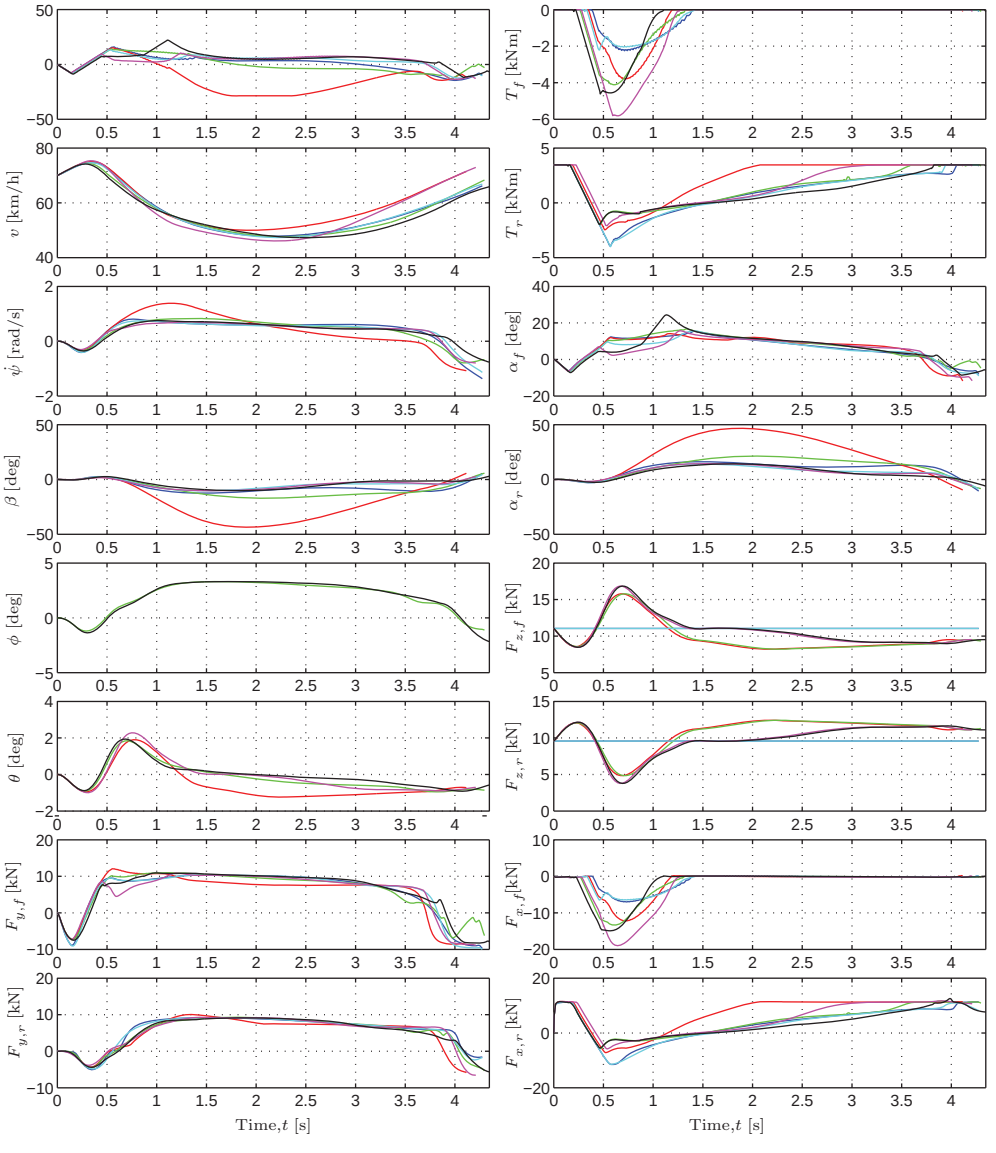

Figure 7. Time-optimal solutions obtained for the 90°-turn, with the respective model configuration. Same colours as in Figure 6. For easier comparison F_x, F_y, T_f, and T_r have been lumped together for the DT models, yielding one longitudinal force, one lateral force, and one torque per axle. In addition, the lateral slip angles are visualised as the mean for the respective axle.

5.3.1. *Geometric trajectories*

The geometric trajectories shown in Figure 6 are similar from a qualitative perspective. The largest discrepancies of the geometric trajectories occur between ST-pitch with FE and ST-pitch with WF during the exit phase, and are approximately 15% of the road width. It is interesting to note that the two ST-pitch configurations result in different strategies when exiting the turn; ST-pitch with WF results in the most narrow curve taking, whereas the ST-pitch with FE results in the most wide. However, irrespective of the tyre model, the differences between the chassis models ST and DT are minor throughout the manoeuvre. Moreover, the

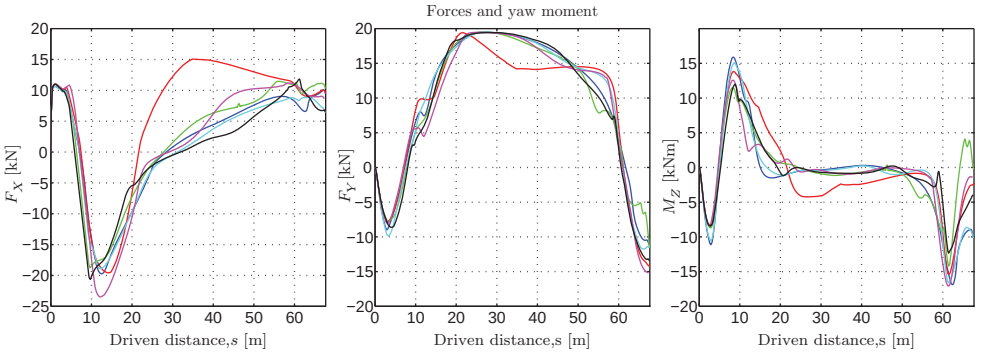

Figure 8. Longitudinal force F_X, lateral force F_Y, and yaw moment M_Z, developed by the tyres in the 90°-turn, illustrated as functions of the driven distance s. Same colours as in Figure 6.

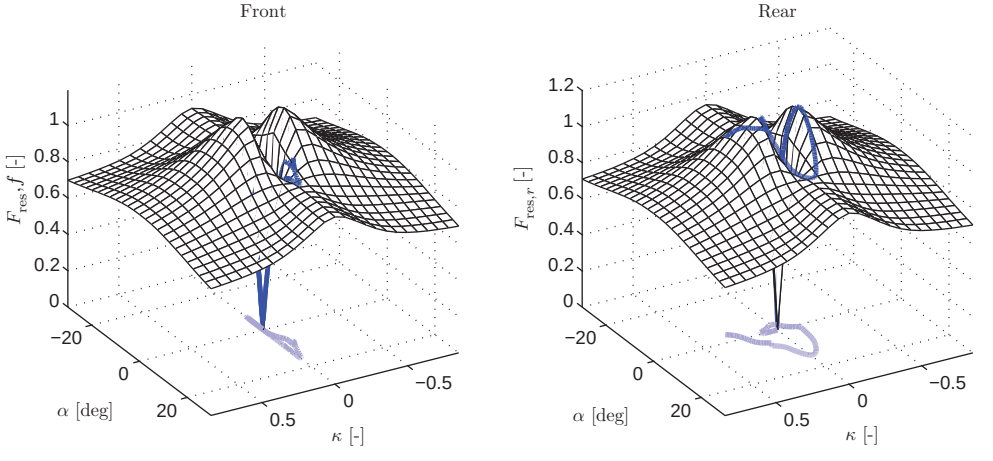

Figure 9. Resultant normalised tyre forces for ST with WF tyre modelling in the 90°-turn.

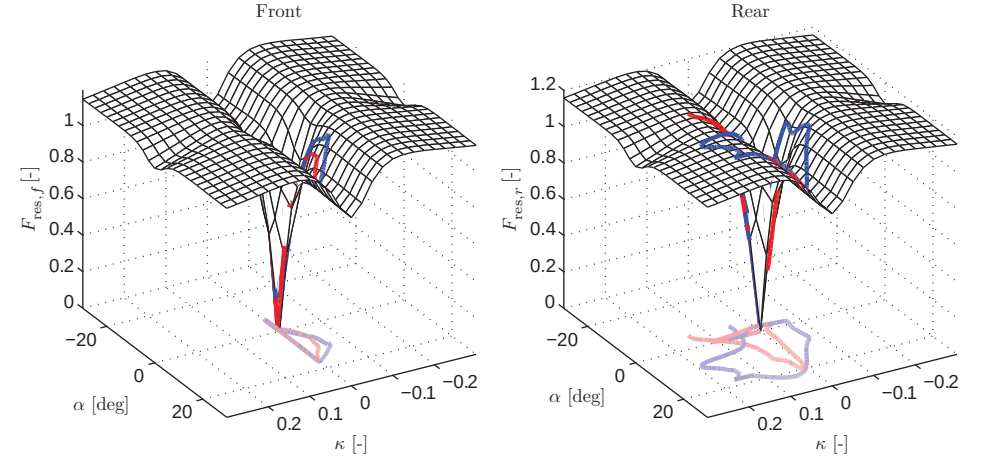

Figure 10. Resultant normalised tyre forces for DT with FE tyre modelling in the 90°-turn (blue – left wheel, red – right wheel).

Table 4. Time for executing the manoeuvre with each model configuration in the 90°-turn.

Model	Manoeuvre execution time (s)
ST FE	4.28
ST WF	4.28
ST-pitch FE	4.12
ST-pitch WF	4.21
DT FE	4.30
DT WF	4.35

geometric paths are virtually indistinguishable for the FE model configurations (even though the slip behaviour is significantly different) but exhibit more variation for the WF tyre models. It is plausible that this is a result of the difference in the tyre force predicted by the respective model for the combined slip; for the FE model, approximately the same tyre force is obtained for different slip combinations. This is not the case for WF, where the tyre force rapidly decreases for increasing slip quantities, and hence the load transfer imposes requirements on the optimal path in the curve taking.

5.3.2. *Trajectories of the model variables*

The first observation when investigating the optimal trajectories for the model variables in Figure 7 closer is that the solution obtained for ST-pitch with FE has a completely different behaviour than the solutions obtained for the other model configurations. In particular, the slip behaviour is much more excessive with this model configuration, which can be observed in the plots for β (peaking at a significant angle of 44°) and α_r. The observed slip behaviour is also consistent with the steering angle, δ, that is computed, where the constraints on the angle are active for a short period around $t = 2$ s. A plausible explanation for this is that the longitudinal load transfer in combination with the characteristics of FE (compare FE and WF in Figure 4) leads to the largest forces that are attained when the vehicle both accelerates and slides. It could also be argued that the longitudinal force is used in the curve for centripetal acceleration, since the friction coefficient in the longitudinal direction is larger than in the lateral direction. For DT, however, heavy centripetal acceleration implies lateral load transfer, resulting in less available tyre force for the inner wheels; thus, limiting the driving/braking effort if wheel spin/lock should be avoided. Disregarding the solution for the ST-pitch with FE and considering all the remaining model configurations, the solutions are similar for several variables, which are ϕ, θ, $\dot{\psi}$, and β.

Investigating the optimal vehicle trajectories further from a qualitative perspective, Figure 7 shows that the different models result in characteristics that are similar in several aspects. Prior to turning towards the corner, all solutions exhibit a slight rightward manoeuvreing while accelerating. This is followed by a braking phase, where both the front and the rear wheels are used. Initially in the braking phase, a significant braking torque is applied, which gradually reduces as the vehicle approaches the turn, see T_f and T_r in Figure 7. Larger lateral forces are generated in the turn. Half-way through the turn, at $t \approx 2$ s, all solutions generate an increasing driving torque, which accelerates the vehicle out of the turn. In the final stage when exiting the turn, all solutions utilise maximum driving torque.

It can be observed that the steer angle varies considerably between the models. At $t \approx 0.7$ s, a smaller δ is obtained for the ST-pitch and DT models with WF for tyre modelling, than for the remaining model configurations. For the ST-pitch and DT models with WF, the longitudinal load transfer is utilised to achieve a strategy with more emphasis on braking

when entering the turn, with the lateral force being slightly smaller. Hence, a lower δ is natural. Shortly after, approximately at $t = 0.8 - 1.2$ s, the steer angle increases sharply in the solutions for the ST-pitch and DT models with WF for tyre modelling. The effect is clearly visible for DT in the front slip angle in Figure 7. This behaviour is not observed for the corresponding models with FE for tyre modelling. Given the resulting forces being developed at the front wheels, at this time there exist two different strategies to achieve the observed behaviour: either by utilising front-wheel braking together with a moderate steering angle, or by only applying a large steer angle and achieve the longitudinal contribution from $F_{y,\mathrm{f}} \sin(\delta)$ solely. The latter seems to be what is utilised for the ST-pitch and DT with WF.

5.3.3. *Tyre forces*

The forces that are developed by the tyres, displayed in Figure 8, mirror the behaviour observed in the internal model variables and geometric trajectory plots; the ST-pitch model with FE exhibits largest discrepancies. Considering the remaining configurations, F_Y and M_Z are similar from a qualitative perspective. The solutions exhibit quantitative differences in the magnitude of M_Z during the initial and exit phases of the manoeuvre. This observation is also in agreement with the tyre-force plots in Figure 7. There are larger numerical discrepancies in F_X, at least during shorter periods of the manoeuvre.

The most prominent differences between the solutions appear, not unexpectedly, for the control inputs and variables closely coupled to the longitudinal dynamics of the vehicle, such as T_f, T_r, and v in Figure 7, and F_X in Figure 8. Comparing the ST models with the DT chassis models, the DT models reduce front-wheel braking slightly earlier, see T_f in Figure 7. This is probably a consequence of T_f being equally distributed between the front wheels for the DT models. Thus, when braking while cornering, the inner wheels will have less load and thus risk to lock up for large braking torques. Similarly, during the exit phase where lateral load transfer still is present, a too large driving torque will spin out the inner rear wheel. Therefore, a smaller driving torque is applied in the solution for DT compared with the optimal solutions for the ST-pitch chassis models in particular.

5.3.4. *FS diagrams*

The FS-diagrams displayed in Figures 9 and 10 for the ST chassis model with WF and for the DT chassis models with FE, respectively, provide further information on the manoeuvre execution. These plots display slightly different slip characteristics for the considered model configurations. For ST, the solver chooses a control strategy such that pure slip is favored, especially for the front wheel. The DT model, having dynamically varying normal forces on the wheels, naturally exhibits different slip trajectories for the left and right wheels. From the FS-diagrams, it is also clear that the slip on the rear wheels is more pronounced as a result of the vehicle being rear-wheel driven.

5.4. *Optimal trajectories in hairpin manoeuvre*

In this section, the time-optimal manoeuvres in the hairpin turn are presented. The analysis of the results for the hairpin manoeuvre is structured in the same manner as for the 90°-turn. The start position in the hairpin turn was $(X_{p,0}, Y_{p,0}) = (-5, 0)$ m for all models, and the initial and final heading angles were aligned with the road direction. Figures 11 and 12 show the vehicle path and the most relevant model variables for all six model configurations in the hairpin manoeuvre. The global forces and yaw moment are displayed in Figure 13, whereas

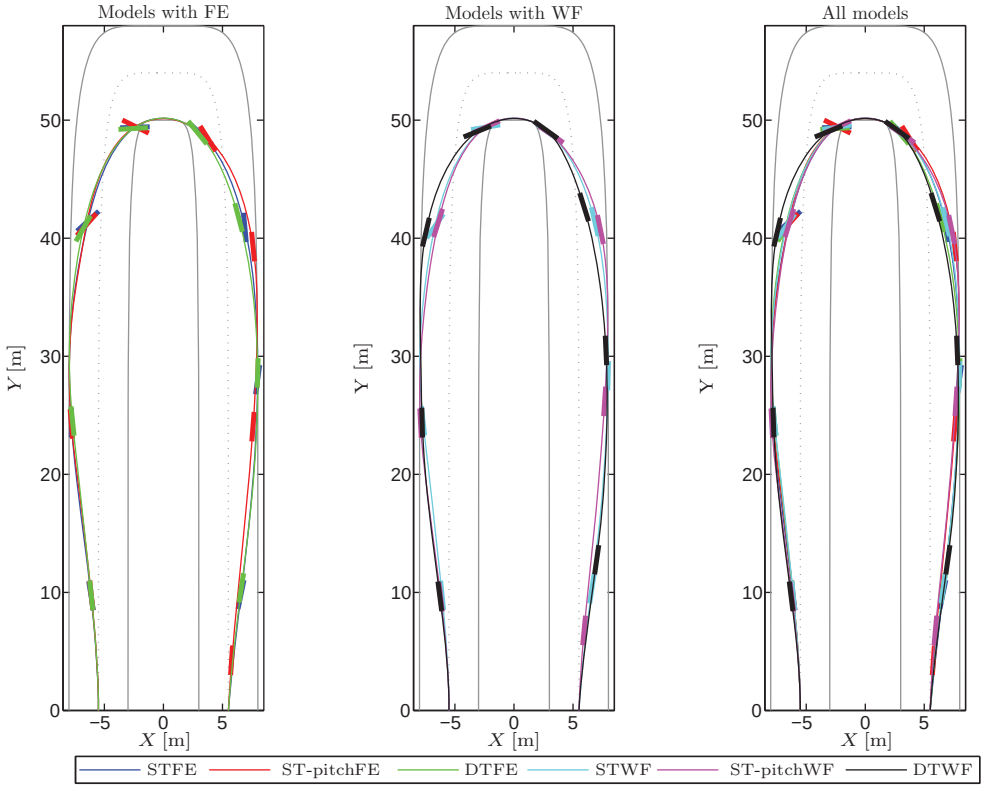

Figure 11. Time-optimal geometric trajectories obtained for the hairpin turn, with the respective model configuration. The coloured bars represent the vehicle heading every second.

the FS-diagrams for the DT chassis model with WF and FE are presented in Figures 14 and 15, respectively. Table 5 displays the manoeuvre execution times achieved with the different model configurations. The objective function t_f deviates approximately 0.4 s when comparing all six model configurations, corresponding to a 5% difference at most. The models with roll and/or pitch dynamics show the largest differences for the respective tyre model, which is caused by additional dynamics leading to large wheel load variations during the manoeuvre. Similarly as for the 90°-turn, the models using FE for tyre modelling have shortest execution times. This is because FE leads to larger resulting forces than WF for combined slip, as can be seen from Figure 4. With load transfer, this difference is even more pronounced. The execution times for ST-pitch are shorter than for the other models. The reason is that the ST-pitch, as does DT, benefits from the longitudinal load transfer when accelerating. However, the ST-pitch does not take roll dynamics into account, whereas a high cornering velocity will result in lateral load transfer caused by the roll dynamics in DT. This leads to reduced loads on the inner wheels for the DT models, which is the same phenomenon as observed in the 90°-turn. Hence, it follows that the execution times will be shorter for the ST-pitch than for both ST and DT.

5.4.1. *Geometric trajectories*

From Figure 11 we see that the geometric paths are qualitatively pairwise equal. For example, the paths for the ST models are rather symmetric in shape. The paths for the ST-pitch and DT models are asymmetric, with the ST-pitch models taking a wide exit out of the turn, and

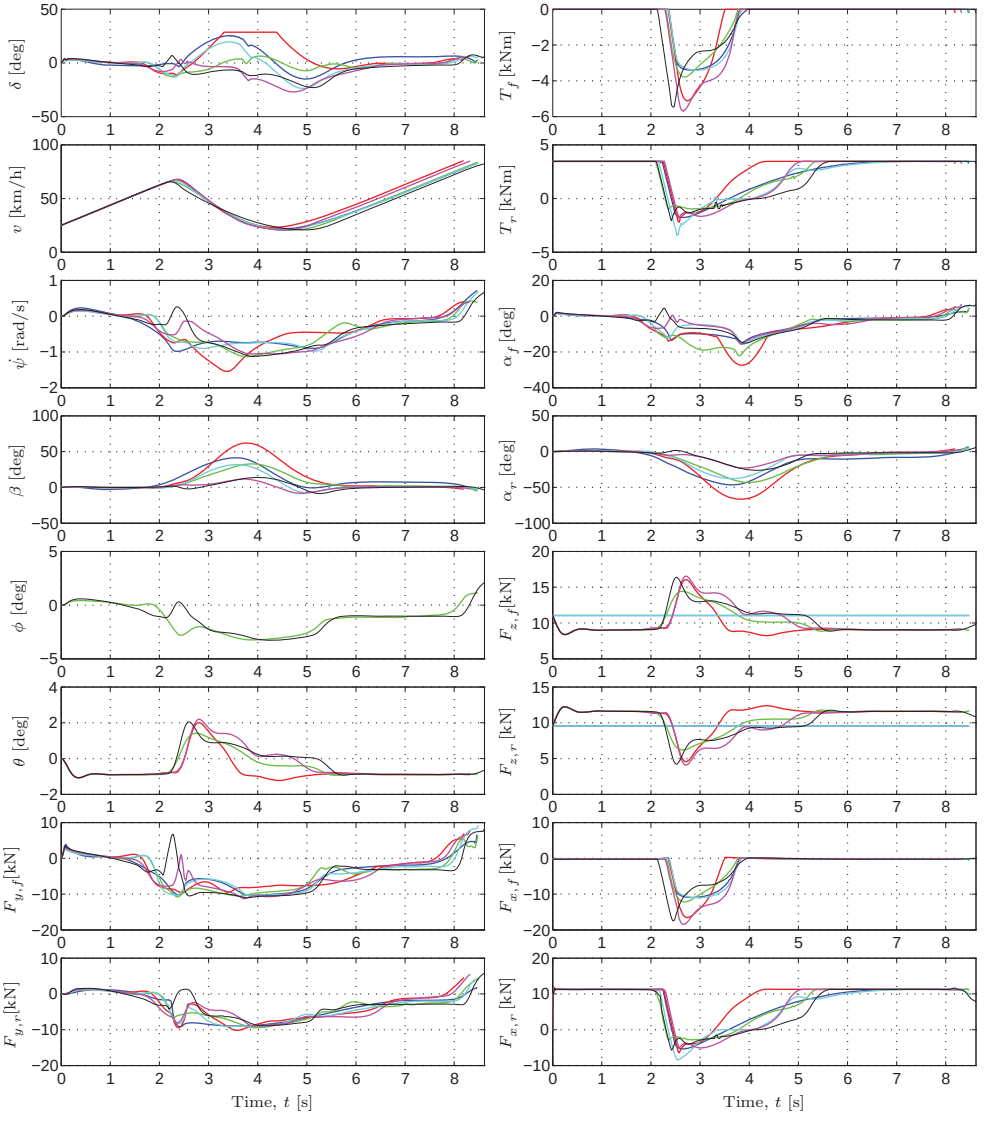

Figure 12. Time-optimal solutions obtained for the hairpin turn, with the respective model configuration. For DT, the total forces and torques on each axle are shown. In addition, the lateral slip angles are visualised as the mean for the respective axle. Same colours as in Figure 11.

opposite for the DT models. The results seem to indicate that the qualitative behaviour is more dependent on the chassis model than the tyre model. However, considering the similarity of the obtained paths for the FE tyre model and the differences in the paths for the WF models (in direct analogy with the results obtained in the 90°-turn), it is clear that the modelling of the tyre forces for large combined slip values is important for the optimal geometric path.

5.4.2. *Trajectories of the model variables*

The trajectories in Figure 12 show that all models have similarities in terms of internal variables: The vehicle starts by giving full driving torque while turning to allow for a wider curve taking. When entering the curve, the vehicle starts to brake with all wheels, which it

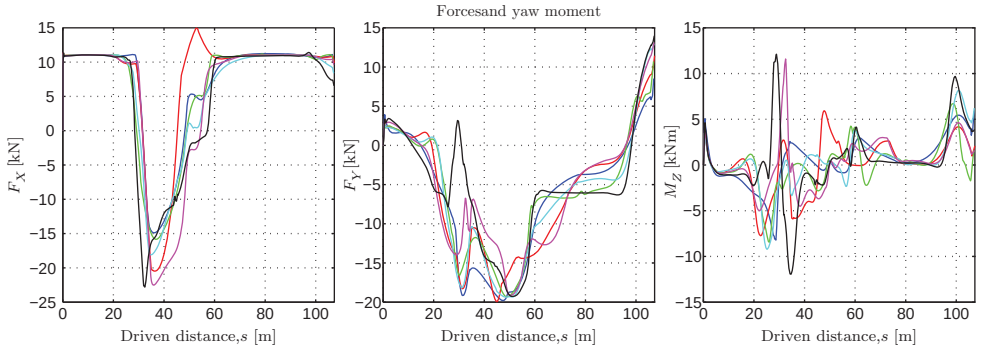

Figure 13. Longitudinal force F_X, lateral force F_Y, and yaw moment M_Z, developed by the tyres in the hairpin turn, illustrated as functions of the driven distance s. Same colours as in Figure 11.

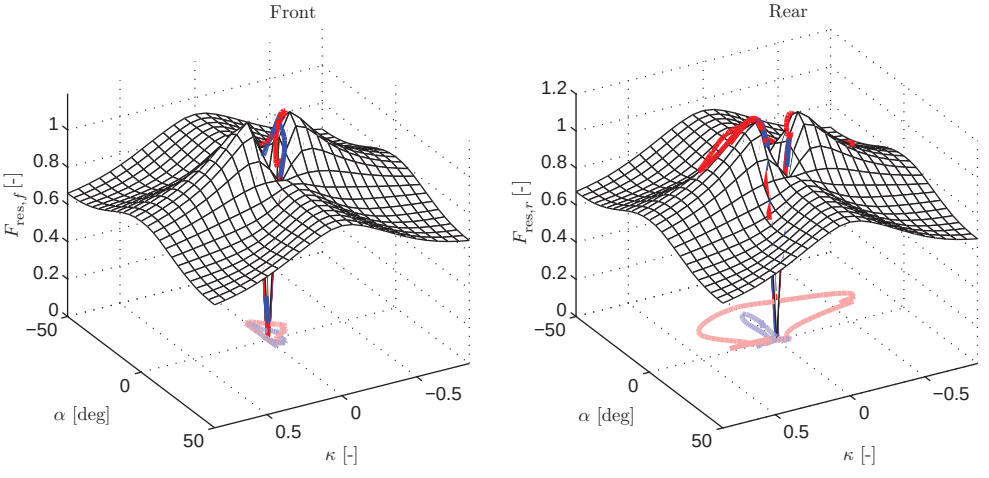

Figure 14. Resultant tyre forces for DT with WF tyre modelling in the hairpin manoeuvre (blue – left wheel, red – right wheel).

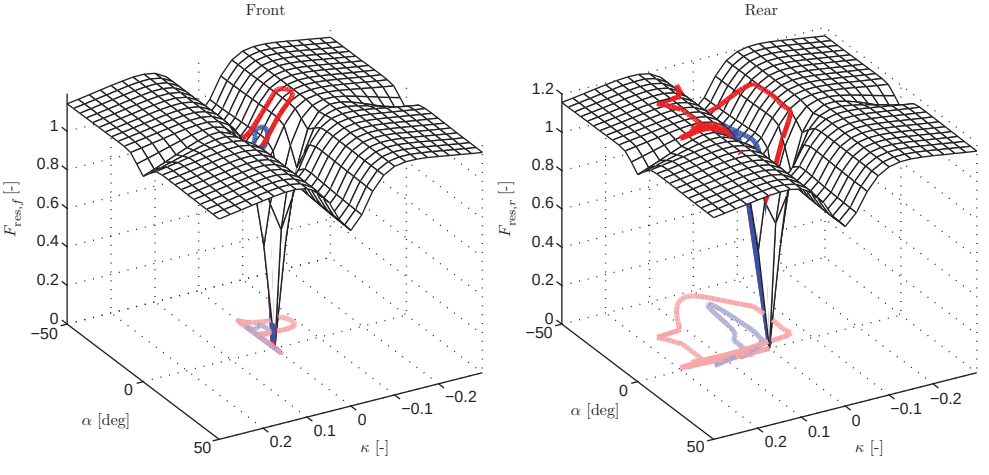

Figure 15. Resultant tyre forces for DT with FE tyre modelling in the hairpin manoeuvre (blue – left wheel, red – right wheel). In contrast to Figure 14, the FE tyre model results in a smaller longitudinal slip but a larger lateral slip. That is, the desired forces are achieved by sliding rather than spinning up or locking the wheels.

Table 5. Time for executing the manoeuvre with each model configuration in the hairpin turn.

Model	Manoeuvre execution time (s)
ST FE	8.47
ST WF	8.49
ST-pitch FE	8.19
ST-pitch WF	8.32
DT FE	8.48
DT WF	8.61

does approximately until reaching the half-way point. Furthermore, all models give rise to vehicle slip. The longitudinal forces and thus also the velocities are also similar in size and shape. However, there are also fundamental differences between the models. Inspecting the body-slip angle, we see that the models with FE have significantly larger slip for the same chassis models, where, for example, β for ST-pitch peaks at approximately 60°. As mentioned previously, the reason why FE gives a larger slip is that the resulting force for FE is higher than that of WF for the combined slip. These differences are coupled to the respective steer angles; δ for ST-pitch with FE at its upper limit for approximately 1 s. For DT, and to some extent the ST-pitch, with WF, there is an abrupt change in δ when reaching the leftmost part of the manoeuvre, at around 2 s. As discussed before, WF results in smaller forces than FE for combined slip. These forces become even smaller for the wheels on the rear axle (especially the rear inner wheel for DT) with longitudinal and/or lateral load transfer, since there will be normal-load variations when cornering and/or braking. Thus, the total decelerating force will be smaller. One way to suppress this is to achieve α_f, α_r that are closer to zero, which can be achieved by the mentioned abrupt change in δ. Neither DT nor ST-pitch with FE exhibit this behaviour, and it is interesting to note that the overall behaviour of DT with FE is similar to the ST models in many variables.

5.4.3. *Tyre forces*

Figure 13 shows the sum of the longitudinal and lateral tyre forces resolved in the road-surface plane as functions of the driven distance. In addition, the yaw moment M_Z generated from the tyre forces is visualised. The qualitative behaviour in the longitudinal forces exhibits similarities for all models, except for the ST-pitch with FE. The behaviour of the lateral forces is also rather similar, even though numerical differences occur. A significant difference is the peak in the lateral force that occurs for DT with WF approximately between $25 < s < 35$ m. This discrepancy is a result of the change in δ discussed earlier. There are qualitative discrepancies between the models in M_Z, where the ST-pitch with WF, DT with WF, and ST-pitch with FE are significantly different in behaviour during the turn part of the manoeuvre. Note that also here the overall behaviour for DT with FE is alike to ST in all three plots, whereas DT with WF is fundamentally different in behaviour during the critical part of the manoeuvre (that is, when in the turn).

5.4.4. *FS diagrams*

Figures 14 and 15 show the FS-diagrams for DT with WF and FE, respectively. It is clear that larger longitudinal slip values are obtained with WF, whereas a higher lateral slip is attained with FE. This observation is related to that for WF, large slip values are required in order to obtain small lateral forces, but for FE, longitudinal slip values of $0.1 - 0.2$ are sufficient

for this purpose. In addition, since the longitudinal force does not depend on the lateral slip in the adopted FE model, in contrast to the WF model, the observed behaviour is expected. With FE, changes in the resulting force seem to have a tendency of moving in orthogonal directions; when altering κ, the lateral slip α hardly changes, and vice versa. However, this is partly a result of that the wheel-torque constraints have been reached (especially for negative slip ratios), and not solely attributed to the FE tyre model.

6. Discussion and conclusions

The time-optimal trajectories in three different time manoeuvres were determined for several vehicle model configurations. Two of them, the 90°-turn and the hairpin turn, were investigated in detail in this paper. The double lane-change manoeuvre provided results that led to similar conclusions as those for the two reported manoeuvres, and this is an important verification that the developed platform can handle a variety of situations relevant for vehicle safety systems. It should also be noted that we have used the same methodology for investigation of the influence on the road surface on the optimal manoeuvre, see [29]. Thus, we believe that the platform is an effective tool for investigation of optimal vehicle manoeuvres and subsequent trajectory generation. Moreover, as, for example, Table 1 shows, it gives a valuable insight into the balance between model detail and computational complexity, which is important for development towards online solutions for optimal vehicle safety systems.

The obtained results provide a solid basis for a discussion of vehicle-model behaviour in time situations. Several interesting properties were found: the differences in behaviour for M_Z between the investigated models are interesting because this variable is often used as a high-level input in safety systems, such as in yaw-rate controllers and rollover-prevention systems. [16,17,26,47] Thus, it seems that the choice of models can potentially lead to fundamentally different control strategies, where, for example, whether to use WF instead of FE with the DT chassis model seems crucial. The characteristics of the two tyre models are fundamentally different. The WF model results in much smaller forces for combined slip compared with when only one of the slip quantities is nonzero. For the FE model, however, the largest forces are attained for the combined slip. It is hard to verify which of the models are the most suitable to use for trajectory generation in extreme manoeuvring. The WF model has been experimentally verified for normal driving conditions on specific road surfaces. However, for large combined slip, we find it hard to explain why the resulting force should be significantly smaller than for pure longitudinal or lateral slip of similar magnitude. Similarly, it is not reasonable that the largest forces should be attained for combined slip, which the FE model predicts as a result of that the longitudinal force is not affected by the lateral slip. Whether to use ST or DT has impact on the employed control strategy. The intuitively obvious choice would be to use DT, because it is a more advanced model. However, the optimal solutions that are obtained indicate that the models with load transfer are highly dependent on the choice of the tyre model, where the different characteristics for combined slip have a larger impact on the solutions. Thus, it is possible that certain combinations of chassis and tyre models are inappropriate and lead to a non-physical behaviour, as surveyed in [4] and discussed in Section 1.

Manoeuvring techniques employed by expert drivers in narrow turns, similar to the hairpin turn, on dry asphalt generally exhibit minor body slip even though individual variations occur. This is, for example, illustrated with measurement data for a rear-wheel-driven vehicle in [12], a front-wheel-driven vehicle in [20], and for an all-wheel-driven vehicle in [10]. If assuming that the driving techniques with a smaller body slip are close to time optimal, it

can be argued that the results obtained with ST-pitch FE, resulting in significant body slip, are not in agreement with reality. Based on this observation, and on the comment regarding inappropriate combinations in the previous paragraph, the ST-pitch models are not considered in the following discussion about the physical consequences in practice.

Considering that the computed time-optimal manoeuvres result in at-the-limit behaviour of the vehicle, we believe that the observations made in this paper have important implications for future safety systems. The solution behaviour is similar in several key aspects for both manoeuvres, as observed in Figures 7 and 12; for example, variables traditionally used for detecting loss of manoeuvring stability, such as the yaw rate, the slip angle, and the roll angle, only show minor discrepancies. The input torques differ significantly during parts of the manoeuvre. In the 90°-turn, however, the overall lateral forces and yaw moments generated by the tyres (see Figure 8) for the considered models have similar characteristics from a qualitative perspective, but with numerical differences in between for certain model configurations. The discrepancies do not have much impact on the other model variables. Moreover, model parameters such as the friction coefficients, vehicle mass, and tyre parameters are uncertain. Hence, safety bounds on supervisory variables have to be set conservatively, for example resulting in early braking in order to surely avoid impact, and the model deviations occurring for low-order models will be suppressed in an online implementation with feedback. The observations are important, because they imply that variables traditionally considered as high-level inputs in safety systems, such as M_Z, may be generated by optimisation using models of low complexity (such as the ST model). These high-level inputs can then be utilised as inputs to a low-level optimiser, which benefits more from complex road interaction models for distributing the desired torque to the respective wheel. This fact, together with the increased amount of sensor data and computational power available in modern road vehicles, opens up for the use of simplistic models when designing the online optimisation-based safety systems of tomorrow.

Funding

This research has been supported by ELLIIT, the Strategic Area for ICT research, funded by the Swedish Government. K. Berntorp and B. Olofsson are members of the LCCC Linnaeus Centre at Lund University, supported by the Swedish Research Council.

Notes

1. Motivated by a passenger vehicle perspective in the analysis, we neglect aerodynamic modelling in the chassis dynamics. It can, however, easily be introduced in the proposed modelling framework if rally or racing applications are to be investigated.
2. In the wheel dynamic modelling, we assume that the vehicle has an open differential, motivated by a passenger-vehicle perspective in the study. However, we have verified that the proposed optimisation framework can handle other differential settings, such as locking differential on the rear axle and limited-slip differential, as well.

References

[1] Isermann R. Fahrdynamik-Regelung: Modellbildung, Fahrerassistenzsysteme, Mechatronik. Wiesbaden: Vieweg-Verlag; 2006.
[2] Liebemann K, Meder K, Schuh J, Nenninger G. Safety and performance enhancement: the Bosch electronic stability control, 2005. Paper Number 05-0471m, Robert Bosch GmbH, Germany.
[3] Funke J, Theodosis P, Hindiyeh R, Stanek G, Kritatakirana K, Gerdes C, Langer D, Hernandez M, Muller-Bessler B, Huhnke B. Up to the limits: autonomous audi TTS. Proc. IEEE Intelligent Vehicles Symp., Alcalá de Henares, Spain; 2012. p. 541–547.

[4] Sharp RS, Peng H. Vehicle dynamics applications of optimal control theory. Veh Syst Dyn. 2011;49:1073–1111.
[5] Pacejka HB. Tire and vehicle dynamics. 2nd ed. Oxford: Butterworth-Heinemann; 2006.
[6] Carlson C, Gerdes J. Consistent nonlinear estimation of longitudinal tire stiffness and effective radius. IEEE Trans Control Syst Technol 2005;13:1010–1020.
[7] Braghin F, Cheli F, Sabbioni E. Environmental effects on Pacejka's scaling factors. Veh Syst Dyn. 2006;44:547–568.
[8] Chakraborty I, Tsiotras P, Diaz RS. Time-optimal vehicle posture control to mitigate unavoidable collisions using conventional control inputs. Proc. Am. Control Conf. (ACC), Washington, DC; 2013. p. 2165–2170.
[9] Esmailzadeh E, Goodarzi A, Vossoughi G. Optimal yaw moment control law for improved vehicle handling. Mechatronics. 2003;13:659–675.
[10] Yi J, Li J, Lu J, Liu Z. On the stability and agility of aggressive vehicle maneuvers: a pendulum-turn maneuver example. IEEE Trans Control Syst Technol. 2012;20:663–676.
[11] Dingle P, Guzzella L. Optimal emergency maneuvers on highways for passenger vehicles with two- and four-wheel active steering. Proc. Am. Control Conf. (ACC), Baltimore, MD; 2010. p. 5374–5381.
[12] Velenis E. FWD vehicle drifting control: the handbrake-cornering technique. Proc. IEEE Conf. Decision and Control (CDC), Orlando, FL; 2011. p. 3258–3263.
[13] Timings JP, Cole DJ. Minimum maneuver time calculation using convex optimization. ASME J Dyn Syst Meas Control. 2013;135:031015-1–031015-9.
[14] Sundström P, Jonasson M, Andreasson J, Stensson Trigell A, Jacobsson B. Path and control optimisation for over-actuated vehicles in two safety- maneuvers. Proc. 10th Int. Symp. Advanced Vehicle Control, Loughborough; 2010.
[15] Andreasson J. Enhancing active safety by extending controllability – How much can be gained? In Proc. IEEE Intelligent Vehicles Symp., China: Xi'an, Shaanxi; 2009. p. 658–662.
[16] Tøndel P, Johansen T. Control allocation for yaw stabilization in automotive vehicles using multiparametric nonlinear programming. In Proc. Am. Control Conf. (ACC), Portland, OR; 2005. p. 453–458.
[17] Schofield B. Model-based vehicle dynamics control for active safety [Ph.D. thesis]. ISRN LUTFD2/TFRT–1083–SE, Department of Automatic Control, Sweden: Lund University; 2008.
[18] Chakraborty I, Tsiotras P, Lu J. Vehicle posture control through aggressive maneuvering for mitigation of t-bone collisions. In Proc. IEEE Conf. Decision and Control (CDC), Orlando, FL; 2011. p. 3264–3269.
[19] Velenis E, Tsiotras P. Minimum time vs. maximum exit velocity path optimization during cornering. Proc. IEEE Int. Symp. Industrial Electronics (ISIE), Croatia: Dubrovnik; 2005. p. 355–360.
[20] Tavernini D, Massaro M, Velenis E, Katzourakis DI, Lot R. Minimum time cornering: the effect of road surface and car transmission layout. Veh Syst Dyn. 2013;51:1533–1547.
[21] Shiller Z, Sundar S. Emergency lane-change maneuvers of autonomous vehicles. ASME J Dyn Syst Meas Control. 1998;120:37–44.
[22] Kelly DP, Sharp RS. Time-optimal control of the race car: a numerical method to emulate the ideal driver. Veh Syst Dyn. 2010;48:1461–1474.
[23] Casanova D. On minimum time vehicle manoeuvring: the theoretical optimal lap [Ph.d. thesis]. Cranfield, Bedforshire: Cranfield University; 2000.
[24] Anderson S, Peters S, Pilutti T, Iagnemma K. An optimal-control-based framework for trajectory planning, threat assessment, and semi-autonomous control of passenger vehicles in hazard avoidance scenarios. Int J Veh Auton Syst. 2010;8:190–216.
[25] Anderson S, Karumanchi S, Iagnemma K. Constraint-based planning and control for safe, semi-autonomous operation of vehicles. In Proc. IEEE Intelligent Vehicles Symp., Spain: Alcalá de Henares; 2012. p. 383–388.
[26] Tjønnås J, Johansen T. Stabilization of automotive vehicles using active steering and adaptive brake control allocation. IEEE Trans Control Syst Technol. 2010;18:545–558.
[27] Berntorp K, Olofsson B, Lundahl K, Bernhardsson B, Nielsen L. Models and methodology for optimal vehicle maneuvers applied to a hairpin turn. Proc. Am. Control Conf. (ACC), Washington, DC; 2013. p. 2139–2146.
[28] Lundahl K, Berntorp K, Olofsson B, Åslund J, Nielsen L. Studying the influence of roll and pitch dynamics in optimal road–vehicle maneuvers. Proc. 23rd Int. Symp. Dynamics of Vehicles on Roads and Tracks (IAVSD), China; Qingdao: 2013.
[29] Olofsson B, Lundahl K, Berntorp K, Nielsen L. An investigation of optimal vehicle maneuvers for different road conditions. Proc. 7th IFAC Symp. Advances in Automotive Control, Tokyo, Japan; 2013. p. 66–71.
[30] Lundahl K, Åslund J, Nielsen L. Vehicle dynamics platform, experiments, and modeling aiming at maneuver handling. Technical Report LiTH-R-3064, Department of Electrical Engineering, Linköpings Universitet, SE-581 83 Linköping, Sweden, 2013.
[31] Berntorp K. Particle filtering and optimal control for vehicles and robots. Sweden: Department of Automatic Control, Lund University; 2014.
[32] Berntorp K. Derivation of a six degrees-of-freedom ground-vehicle model for automotive applications. Technical Report ISRN LUTFD2/TFRT–7627–SE, Department of Automatic Control, Sweden: Lund University; 2013.
[33] Schindler E. Fahrdynamik: Grundlagen Des Lenkverhaltens Und Ihre Anwendung Für Fahrzeugregelsysteme. Renningen: Expert-Verlag; 2007.
[34] Kiencke U, Nielsen L. Automotive control systems – for engine, driveline and vehicle. 2nd ed. Berlin: Springer-Verlag; 2005.
[35] Rajamani R. Vehicle dynamics and control. Berlin: Springer-Verlag, 2006.

[36] Wong J. Theory of ground vehicles. Hoboken, NJ: John Wiley & Sons; 2008.
[37] Modelica Association . Available from: http://www.modelica.org.
[38] Åkesson J. Optimica – an extension of modelica supporting dynamic optimization. Proc. 6th Int. Modelica Conf., Bielefeld; 2008. p. 57–66.
[39] Biegler LT, Cervantes AM, Wächter A. Advances in simultaneous strategies for dynamic process optimization. Chem Eng Sci. 2002;57:575–593.
[40] Åkesson J. Languages and tools for optimization of large-scale systems [Ph.D. thesis]. ISRN LUTFD2/TFRT–1081–SE, Sweden: Department of Automatic Control, Lund University; 2007.
[41] Wächter A, Biegler LT. On the implementation of an interior-point filter line-search algorithm for large-scale nonlinear programming. Math Program. 2006;106:25–57.
[42] Åkesson J, Årzén KE, Gäfvert M, Bergdahl T, Tummescheit H. Modeling and optimization with optimica and jmodelica.org – languages and tools for solving large-scale dynamic optimization problems. Comput Chem Eng. 2010;34:1737–1749.
[43] JModelica.org . Available from: http://www.jmodelica.org
[44] Dennis J, Schnabel R. Numerical methods for unconstrained optimization and nonlinear equations. Classics in Applied Mathematics, Society for Industrial and Applied Mathematics, 1983.
[45] Griewank A. Evaluating derivatives: principles and techniques of algorithmic differentiation. Frontiers Appl Math. Philadelphia (PA): SIAM; 2000.
[46] ISO 3888-2:2011. Passenger cars – test track for a severe lane-change manoeuvre – Part 2: obstacle avoidance. International Organization for Standardization, Geneva, Switzerland; 2011.
[47] Berntorp K. ESP for suppression of jackknifing in an articulated bus [Master's thesis]. ISRN LUTFD2/TFRT–5831–SE, Department of Automatic Control, Sweden: Lund University; 2008.